

Measurement of Singly Cabibbo Suppressed Decays $\Lambda_c^+ \rightarrow p\pi^+\pi^-$ and $\Lambda_c^+ \rightarrow pK^+K^-$

M. Ablikim¹, M. N. Achasov^{9,e}, S. Ahmed¹⁴, X. C. Ai¹, O. Albayrak⁵, M. Albrecht⁴, D. J. Ambrose⁴⁴, A. Amoroso^{49A,49C}, F. F. An¹, Q. An^{46,a}, J. Z. Bai¹, O. Bakina²³, R. Baldini Ferroli^{20A}, Y. Ban³¹, D. W. Bennett¹⁹, J. V. Bennett⁵, N. Berger²², M. Bertani^{20A}, D. Bettoni^{21A}, J. M. Bian⁴³, F. Bianchi^{49A,49C}, E. Boger^{23,c}, I. Boyko²³, R. A. Briere⁵, H. Cai⁵¹, X. Cai^{1,a}, O. Cakir^{40A}, A. Calcaterra^{20A}, G. F. Cao¹, S. A. Cetin^{40B}, J. Chai^{49C}, J. F. Chang^{1,a}, G. Chelkov^{23,c,d}, G. Chen¹, H. S. Chen¹, J. C. Chen¹, M. L. Chen^{1,a}, S. Chen⁴¹, S. J. Chen²⁹, X. Chen^{1,a}, X. R. Chen²⁶, Y. B. Chen^{1,a}, H. P. Cheng¹⁷, X. K. Chu³¹, G. Cibinetto^{21A}, H. L. Dai^{1,a}, J. P. Dai³⁴, A. Dbeyssi¹⁴, D. Dedovich²³, Z. Y. Deng¹, A. Denig²², I. Denysenko²³, M. Destefanis^{49A,49C}, F. De Mori^{49A,49C}, Y. Ding²⁷, C. Dong³⁰, J. Dong^{1,a}, L. Y. Dong¹, M. Y. Dong^{1,a}, Z. L. Dou²⁹, S. X. Du⁵³, P. F. Duan¹, J. Z. Fan³⁹, J. Fang^{1,a}, S. S. Fang¹, X. Fang^{46,a}, Y. Fang¹, R. Farinelli^{21A,21B}, L. Fava^{49B,49C}, S. Fegan²², F. Feldbauer²², G. Felici^{20A}, C. Q. Feng^{46,a}, E. Fioravanti^{21A}, M. Fritsch^{14,22}, C. D. Fu¹, Q. Gao¹, X. L. Gao^{46,a}, Y. Gao³⁹, Z. Gao^{46,a}, I. Garzia^{21A}, K. Goetzen¹⁰, L. Gong³⁰, W. X. Gong^{1,a}, W. Gradl²², M. Greco^{49A,49C}, M. H. Gu^{1,a}, Y. T. Gu¹², Y. H. Guan¹, A. Q. Guo¹, L. B. Guo²⁸, R. P. Guo¹, Y. Guo¹, Y. P. Guo²², Z. Haddadi²⁵, A. Hafner²², S. Han⁵¹, X. Q. Hao¹⁵, F. A. Harris⁴², K. L. He¹, F. H. Heinsius⁴, T. Held⁴, Y. K. Heng^{1,a}, T. Holtmann⁴, Z. L. Hou¹, C. Hu²⁸, H. M. Hu¹, J. F. Hu^{49A,49C}, T. Hu^{1,a}, Y. Hu¹, G. S. Huang^{46,a}, J. S. Huang¹⁵, X. T. Huang³³, X. Z. Huang²⁹, Y. Huang²⁹, Z. L. Huang²⁷, T. Hussain⁴⁸, W. Ikegami Andersson⁵⁰, Q. Ji¹, Q. P. Ji¹⁵, X. B. Ji¹, X. L. Ji^{1,a}, L. W. Jiang⁵¹, X. S. Jiang^{1,a}, X. Y. Jiang³⁰, J. B. Jiao³³, Z. Jiao¹⁷, D. P. Jin^{1,a}, S. Jin¹, T. Johansson⁵⁰, A. Julin⁴³, N. Kalantar-Nayestanaki²⁵, X. L. Kang¹, X. S. Kang³⁰, M. Kavatsyuk²⁵, B. C. Ke⁵, P. Kiese²², R. Kliemt¹⁰, B. Kloss²², O. B. Kolcu^{40B,h}, B. Kopf⁴, M. Kornicer⁴², A. Kupsc⁵⁰, W. Kühn²⁴, J. S. Lange²⁴, M. Lara¹⁹, P. Larin¹⁴, H. Leithoff²², C. Leng^{49C}, C. Li⁵⁰, Cheng Li^{46,a}, D. M. Li⁵³, F. Li^{1,a}, F. Y. Li³¹, G. Li¹, H. B. Li¹, H. J. Li¹, J. C. Li¹, Jin Li³², K. Li³³, K. Li¹³, Lei Li³, P. L. Li^{46,a}, P. R. Li⁴¹, Q. Y. Li³³, T. Li³³, W. D. Li¹, W. G. Li¹, X. L. Li³³, X. N. Li^{1,a}, X. Q. Li³⁰, Y. B. Li², Z. B. Li³⁸, H. Liang^{46,a}, Y. F. Liang³⁶, Y. T. Liang²⁴, G. R. Liao¹¹, D. X. Lin¹⁴, B. Liu³⁴, B. J. Liu¹, C. X. Liu¹, D. Liu^{46,a}, F. H. Liu³⁵, Fang Liu¹, Feng Liu⁶, H. B. Liu¹², H. H. Liu¹, H. H. Liu¹⁶, H. M. Liu¹, J. Liu¹, J. B. Liu^{46,a}, J. P. Liu⁵¹, J. Y. Liu¹, K. Liu³⁹, K. Y. Liu²⁷, L. D. Liu³¹, P. L. Liu^{1,a}, Q. Liu⁴¹, S. B. Liu^{46,a}, X. Liu²⁶, Y. B. Liu³⁰, Y. Y. Liu³⁰, Z. A. Liu^{1,a}, Zhiqing Liu²², H. Loehner²⁵, Y. F. Long³¹, X. C. Lou^{1,a,g}, H. J. Lu¹⁷, J. G. Lu^{1,a}, Y. Lu¹, Y. P. Lu^{1,a}, C. L. Luo²⁸, M. X. Luo⁵², T. Luo⁴², X. L. Luo^{1,a}, X. R. Lyu⁴¹, F. C. Ma²⁷, H. L. Ma¹, L. L. Ma³³, M. M. Ma¹, Q. M. Ma¹, T. Ma¹, X. N. Ma³⁰, X. Y. Ma^{1,a}, Y. M. Ma³³, F. E. Maas¹⁴, M. Maggiora^{49A,49C}, Q. A. Malik⁴⁸, Y. J. Mao³¹, Z. P. Mao¹, S. Marcello^{49A,49C}, J. G. Messchendorp²⁵, G. Mezzadri^{21B}, J. Min^{1,a}, T. J. Min¹, R. E. Mitchell¹⁹, X. H. Mo^{1,a}, Y. J. Mo⁶, C. Morales Morales¹⁴, N. Yu. Muchnoi^{9,e}, H. Muramatsu⁴³, P. Musiol⁴, Y. Nefedov²³, F. Nerling¹⁰, I. B. Nikolaev^{9,e}, Z. Ning^{1,a}, S. Nisar⁸, S. L. Niu^{1,a}, X. Y. Niu¹, S. L. Olsen³², Q. Ouyang^{1,a}, S. Pacetti^{20B}, Y. Pan^{46,a}, P. Patteri^{20A}, M. Pelizaeus⁴, H. P. Peng^{46,a}, K. Peters^{10,i}, J. Pettersson⁵⁰, J. L. Ping²⁸, R. G. Ping¹, R. Poling⁴³, V. Prasad¹, H. R. Qi², M. Qi²⁹, S. Qian^{1,a}, C. F. Qiao⁴¹, L. Q. Qin³³, N. Qin⁵¹, X. S. Qin¹, Z. H. Qin^{1,a}, J. F. Qiu¹, K. H. Rashid⁴⁸, C. F. Redmer²², M. Ripka²², G. Rong¹, Ch. Rosner¹⁴, X. D. Ruan¹², A. Sarantsev^{23,f}, M. Savrié^{21B}, C. Schnier⁴, K. Schoenning⁵⁰, S. Schumann²², W. Shan³¹, M. Shao^{46,a}, C. P. Shen², P. X. Shen³⁰, X. Y. Shen¹, H. Y. Sheng¹, M. Shi¹, W. M. Song¹, X. Y. Song¹, S. Sosio^{49A,49C}, S. Spataro^{49A,49C}, G. X. Sun¹, J. F. Sun¹⁵, S. S. Sun¹, X. H. Sun¹, Y. J. Sun^{46,a}, Y. Z. Sun¹, Z. J. Sun^{1,a}, Z. T. Sun¹⁹, C. J. Tang³⁶, X. Tang¹, I. Tapan^{40C}, E. H. Thorndike⁴⁴, M. Tiemens²⁵, I. Uman^{40D}, G. S. Varner⁴², B. Wang³⁰, B. L. Wang⁴¹, D. Wang³¹, D. Y. Wang³¹, K. Wang^{1,a}, L. L. Wang¹, L. S. Wang¹, M. Wang³³, P. Wang¹, P. L. Wang¹, W. Wang^{1,a}, W. P. Wang^{46,a}, X. F. Wang³⁹, Y. Wang³⁷, Y. D. Wang¹⁴, Y. F. Wang^{1,a}, Y. Q. Wang²², Z. Wang^{1,a}, Z. G. Wang^{1,a}, Z. H. Wang^{46,a}, Z. Y. Wang¹, Z. Y. Wang¹, T. Weber²², D. H. Wei¹¹, P. Weidenkaff²², S. P. Wen¹, U. Wiedner⁴, M. Wolke⁵⁰, L. H. Wu¹, L. J. Wu¹, Z. Wu^{1,a}, L. Xia^{46,a}, L. G. Xia³⁹, Y. Xia¹⁸, D. Xiao¹, H. Xiao⁴⁷, Z. J. Xiao²⁸, Y. G. Xie^{1,a}, Q. L. Xiu^{1,a}, G. F. Xu¹, J. J. Xu¹, L. Xu¹, Q. J. Xu¹³, Q. N. Xu⁴¹, X. P. Xu³⁷, L. Yan^{49A,49C}, W. B. Yan^{46,a}, W. C. Yan^{46,a}, Y. H. Yan¹⁸, H. J. Yang^{34,j}, H. X. Yang¹, L. Yang⁵¹, Y. X. Yang¹¹, M. Ye^{1,a}, M. H. Ye⁷, J. H. Yin¹, Z. Y. You³⁸, B. X. Yu^{1,a}, C. X. Yu³⁰, J. S. Yu²⁶, C. Z. Yuan¹, W. L. Yuan²⁹, Y. Yuan¹, A. Yuncu^{40B,b}, A. A. Zafar⁴⁸, A. Zallo^{20A}, Y. Zeng¹⁸, Z. Zeng^{46,a}, B. X. Zhang¹, B. Y. Zhang^{1,a}, C. Zhang²⁹, C. C. Zhang¹, D. H. Zhang¹, H. H. Zhang³⁸, H. Y. Zhang^{1,a}, J. Zhang¹, J. J. Zhang¹, J. L. Zhang¹, J. Q. Zhang¹, J. W. Zhang^{1,a}, J. Y. Zhang¹, J. Z. Zhang¹, K. Zhang¹, L. Zhang¹, S. Q. Zhang³⁰, X. Y. Zhang³³, Y. Zhang¹, Y. Zhang¹, Y. H. Zhang^{1,a}, Y. N. Zhang⁴¹, Y. T. Zhang^{46,a}, Yu Zhang⁴¹, Z. H. Zhang⁶, Z. P. Zhang⁴⁶, Z. Y. Zhang⁵¹, G. Zhao¹, J. W. Zhao^{1,a}, J. Y. Zhao¹, J. Z. Zhao^{1,a}, Lei Zhao^{46,a}, Ling Zhao¹, M. G. Zhao³⁰, Q. Zhao¹, Q. W. Zhao¹, S. J. Zhao⁵³, T. C. Zhao¹, Y. B. Zhao^{1,a}, Z. G. Zhao^{46,a}, A. Zhemchugov^{23,c}, B. Zheng⁴⁷, J. P. Zheng^{1,a}, W. J. Zheng³³, Y. H. Zheng⁴¹, B. Zhong²⁸, L. Zhou^{1,a}, X. Zhou⁵¹, X. K. Zhou^{46,a}, X. R. Zhou^{46,a}, X. Y. Zhou¹, K. Zhu¹, K. J. Zhu^{1,a}, S. Zhu¹, S. H. Zhu⁴⁵,

X. L. Zhu³⁹, Y. C. Zhu^{46,a}, Y. S. Zhu¹, Z. A. Zhu¹, J. Zhuang^{1,a}, L. Zotti^{49A,49C}, B. S. Zou¹, J. H. Zou¹

(BESIII Collaboration)

- ¹ *Institute of High Energy Physics, Beijing 100049, People's Republic of China*
² *Beihang University, Beijing 100191, People's Republic of China*
³ *Beijing Institute of Petrochemical Technology, Beijing 102617, People's Republic of China*
⁴ *Bochum Ruhr-University, D-44780 Bochum, Germany*
⁵ *Carnegie Mellon University, Pittsburgh, Pennsylvania 15213, USA*
⁶ *Central China Normal University, Wuhan 430079, People's Republic of China*
⁷ *China Center of Advanced Science and Technology, Beijing 100190, People's Republic of China*
⁸ *COMSATS Institute of Information Technology, Lahore, Defence Road, Off Raiwind Road, 54000 Lahore, Pakistan*
⁹ *G.I. Budker Institute of Nuclear Physics SB RAS (BINP), Novosibirsk 630090, Russia*
¹⁰ *GSI Helmholtz Centre for Heavy Ion Research GmbH, D-64291 Darmstadt, Germany*
¹¹ *Guangxi Normal University, Guilin 541004, People's Republic of China*
¹² *Guangxi University, Nanning 530004, People's Republic of China*
¹³ *Hangzhou Normal University, Hangzhou 310036, People's Republic of China*
¹⁴ *Helmholtz Institute Mainz, Johann-Joachim-Becher-Weg 45, D-55099 Mainz, Germany*
¹⁵ *Henan Normal University, Xinxiang 453007, People's Republic of China*
¹⁶ *Henan University of Science and Technology, Luoyang 471003, People's Republic of China*
¹⁷ *Huangshan College, Huangshan 245000, People's Republic of China*
¹⁸ *Hunan University, Changsha 410082, People's Republic of China*
¹⁹ *Indiana University, Bloomington, Indiana 47405, USA*
²⁰ *(A)INFN Laboratori Nazionali di Frascati, I-00044, Frascati, Italy; (B)INFN and University of Perugia, I-06100, Perugia, Italy*
²¹ *(A)INFN Sezione di Ferrara, I-44122, Ferrara, Italy; (B)University of Ferrara, I-44122, Ferrara, Italy*
²² *Johannes Gutenberg University of Mainz, Johann-Joachim-Becher-Weg 45, D-55099 Mainz, Germany*
²³ *Joint Institute for Nuclear Research, 141980 Dubna, Moscow region, Russia*
²⁴ *Justus-Liebig-Universitaet Giessen, II. Physikalisches Institut, Heinrich-Buff-Ring 16, D-35392 Giessen, Germany*
²⁵ *KVI-CART, University of Groningen, NL-9747 AA Groningen, The Netherlands*
²⁶ *Lanzhou University, Lanzhou 730000, People's Republic of China*
²⁷ *Liaoning University, Shenyang 110036, People's Republic of China*
²⁸ *Nanjing Normal University, Nanjing 210023, People's Republic of China*
²⁹ *Nanjing University, Nanjing 210093, People's Republic of China*
³⁰ *Nankai University, Tianjin 300071, People's Republic of China*
³¹ *Peking University, Beijing 100871, People's Republic of China*
³² *Seoul National University, Seoul, 151-747 Korea*
³³ *Shandong University, Jinan 250100, People's Republic of China*
³⁴ *Shanghai Jiao Tong University, Shanghai 200240, People's Republic of China*
³⁵ *Shanxi University, Taiyuan 030006, People's Republic of China*
³⁶ *Sichuan University, Chengdu 610064, People's Republic of China*
³⁷ *Soochow University, Suzhou 215006, People's Republic of China*
³⁸ *Sun Yat-Sen University, Guangzhou 510275, People's Republic of China*
³⁹ *Tsinghua University, Beijing 100084, People's Republic of China*
⁴⁰ *(A)Ankara University, 06100 Tandogan, Ankara, Turkey; (B)Istanbul Bilgi University, 34060 Eyup, Istanbul, Turkey; (C)Uludag University, 16059 Bursa, Turkey; (D)Near East University, Nicosia, North Cyprus, Mersin 10, Turkey*
⁴¹ *University of Chinese Academy of Sciences, Beijing 100049, People's Republic of China*
⁴² *University of Hawaii, Honolulu, Hawaii 96822, USA*
⁴³ *University of Minnesota, Minneapolis, Minnesota 55455, USA*
⁴⁴ *University of Rochester, Rochester, New York 14627, USA*
⁴⁵ *University of Science and Technology Liaoning, Anshan 114051, People's Republic of China*
⁴⁶ *University of Science and Technology of China, Hefei 230026, People's Republic of China*
⁴⁷ *University of South China, Hengyang 421001, People's Republic of China*
⁴⁸ *University of the Punjab, Lahore-54590, Pakistan*

⁴⁹ (A)University of Turin, I-10125, Turin, Italy; (B)University of Eastern Piedmont, I-15121, Alessandria, Italy; (C)INFN, I-10125, Turin, Italy

⁵⁰ Uppsala University, Box 516, SE-75120 Uppsala, Sweden

⁵¹ Wuhan University, Wuhan 430072, People's Republic of China

⁵² Zhejiang University, Hangzhou 310027, People's Republic of China

⁵³ Zhengzhou University, Zhengzhou 450001, People's Republic of China

^a Also at State Key Laboratory of Particle Detection and Electronics, Beijing 100049, Hefei 230026, People's Republic of China

^b Also at Bogazici University, 34342 Istanbul, Turkey

^c Also at the Moscow Institute of Physics and Technology, Moscow 141700, Russia

^d Also at the Functional Electronics Laboratory, Tomsk State University, Tomsk, 634050, Russia

^e Also at the Novosibirsk State University, Novosibirsk, 630090, Russia

^f Also at the NRC "Kurchatov Institute", PNPI, 188300, Gatchina, Russia

^g Also at University of Texas at Dallas, Richardson, Texas 75083, USA

^h Also at Istanbul Arel University, 34295 Istanbul, Turkey

ⁱ Also at Goethe University Frankfurt, 60323 Frankfurt am Main, Germany

^j Also at Institute of Nuclear and Particle Physics, Shanghai Key Laboratory for Particle Physics and Cosmology, Shanghai 200240, People's Republic of China

(Dated: March 8, 2022)

Using 567 pb⁻¹ of data collected with the BESIII detector at a center-of-mass energy of $\sqrt{s} = 4.599$ GeV, near the $\Lambda_c^+ \bar{\Lambda}_c^-$ threshold, we study the singly Cabibbo-suppressed decays $\Lambda_c^+ \rightarrow p\pi^+\pi^-$ and $\Lambda_c^+ \rightarrow pK^+K^-$. By normalizing with respect to the Cabibbo-favored decay $\Lambda_c^+ \rightarrow pK^-\pi^+$, we obtain ratios of branching fractions: $\frac{\mathcal{B}(\Lambda_c^+ \rightarrow p\pi^+\pi^-)}{\mathcal{B}(\Lambda_c^+ \rightarrow pK^-\pi^+)} = (6.70 \pm 0.48 \pm 0.25)\%$, $\frac{\mathcal{B}(\Lambda_c^+ \rightarrow p\phi)}{\mathcal{B}(\Lambda_c^+ \rightarrow pK^-\pi^+)} = (1.81 \pm 0.33 \pm 0.13)\%$, and $\frac{\mathcal{B}(\Lambda_c^+ \rightarrow pK^+K_{\text{non-}\phi}^-)}{\mathcal{B}(\Lambda_c^+ \rightarrow pK^-\pi^+)} = (9.36 \pm 2.22 \pm 0.71) \times 10^{-3}$, where the uncertainties are statistical and systematic, respectively. The absolute branching fractions are also presented. Among these measurements, the decay $\Lambda_c^+ \rightarrow p\pi^+\pi^-$ is observed for the first time, and the precision of the branching fraction for $\Lambda_c^+ \rightarrow pK^+K_{\text{non-}\phi}^-$ and $\Lambda_c^+ \rightarrow p\phi$ is significantly improved.

PACS numbers: 14.20.Lq, 13.30.Eg, 13.66.Bc, 12.38.Qk

Hadronic decays of charmed baryons provide an ideal laboratory to understand the interplay of weak and strong interaction in the charm region [1–9], which is complementary to charmed mesons. They also provide essential input for studying the decays of b -flavored hadrons involving a Λ_c in the final state [10, 11]. In contrast to the charmed meson decays, which are usually dominated by factorizable amplitudes, decays of charmed baryons receive sizable nonfactorizable contributions from W -exchange diagrams, which are subject to color and helicity suppression. The study of nonfactorizable contributions is critical to understand the dynamics of charmed baryon decays.

Since the first discovery of the ground state charmed baryon Λ_c in 1979 [12, 13], progress with charmed baryons has been relatively slow, due to a scarcity of experimental data. Recently, based on an e^+e^- annihilation data sample of 567 pb⁻¹ [14] at a center-of-mass (c.m.) energy of $\sqrt{s} = 4.599$ GeV, the BESIII Collaboration measured the absolute branching fractions (BFs) of 12 Cabibbo-favored (CF) Λ_c^+ hadronic decays with a significantly improved precision [15]. For many other CF charmed baryon decay modes and most of the singly Cabibbo-suppressed (SCS) decays, however, no precision measurements are available; many of them even

have not yet been measured [16]. As a consequence, we are not able to distinguish between the theoretical predictions among the different models [3–9].

The SCS decays $\Lambda_c^+ \rightarrow p\pi^+\pi^-$ and $\Lambda_c^+ \rightarrow pK^+K^-$ proceed via the external W -emission, internal W -emission and W -exchange processes. Precisely measuring and comparing their BFs may help to reveal the Λ_c internal dynamics [1]. A measurement of the SCS mode $\Lambda_c^+ \rightarrow p\phi$ is of particular interest because it receives contributions only from the internal W -emission diagrams, which can reliably be obtained by a factorization approach [1]. An improved measurement of the $\Lambda_c^+ \rightarrow p\phi$ BF is thus essential to validate theoretical models and test the application of large- N_c factorization in the charmed baryon sector [17], where, N_c is the number of colors.

In this Letter, we describe a search for the SCS decays $\Lambda_c^+ \rightarrow p\pi^+\pi^-$ and present an improved measurement of the $\Lambda_c^+ \rightarrow pK^+K_{\text{non-}\phi}^-$ and $\Lambda_c^+ \rightarrow p\phi$ BFs. The BFs are measured relative to the CF mode $\Lambda_c^+ \rightarrow pK^-\pi^+$. Our analysis is based on the same data sample as that used in Ref. [15] collected by the BESIII detector. Details on the features and capabilities of the BESIII detector can be found in Ref. [18]. Throughout this Letter, charge-

conjugate modes are implicitly included, unless otherwise stated.

The GEANT4-based [19] Monte Carlo (MC) simulations of e^+e^- annihilations are used to understand the backgrounds and to estimate detection efficiencies. The generator KKMC [20] is used to simulate the beam-energy spread and initial-state radiation (ISR) of the e^+e^- collisions. The inclusive MC sample includes $\Lambda_c^+\bar{\Lambda}_c^-$ events, charmed meson $D_{(s)}^{(*)}$ pair production, ISR returns to lower-mass ψ states, and continuum processes $e^+e^- \rightarrow q\bar{q}$ ($q = u, d, s$). Decay modes as specified in the PDG [16] are modeled with EVTGEN [21, 22]. Signal MC samples of $e^+e^- \rightarrow \Lambda_c^+\bar{\Lambda}_c^-$ are produced in which the Λ_c^+ decays to the interested final state ($pK^-\pi^+$, $p\pi^+\pi^-$, or pK^+K^-) together with the $\bar{\Lambda}_c^-$ decaying generically to all possible final states.

Charged tracks are reconstructed from hits in the main drift chamber (MDC) and are required to have polar angles within $|\cos\theta| < 0.93$. The points of closest approach of the charged tracks to the interaction point (IP) are required to be within 1 cm in the plane perpendicular to the beam (V_r) and ± 10 cm along the beam (V_z). Information from the time-of-flight (TOF) system and dE/dx in the MDC are combined to form PID confidence levels (C.L.) for the π , K and p hypotheses. Each track is assigned to the particle type with the highest particle identification (PID) C.L. To avoid backgrounds from beam interactions with residual gas or detector materials (beam pipe and MDC inner wall), a further requirement of $V_r < 0.2$ cm is imposed for the proton.

Λ_c^+ candidates are reconstructed by considering all combinations of charged tracks in the final states of interest $pK^-\pi^+$, $p\pi^+\pi^-$, and pK^+K^- . Two variables, the energy difference $\Delta E = E - E_{\text{beam}}$ and the beam-constrained mass $M_{\text{BC}} = \sqrt{E_{\text{beam}}^2/c^4 - p^2/c^2}$, are used to identify the Λ_c^+ candidates. Here, E_{beam} is the beam energy, and $E(p)$ is the reconstructed energy (momentum) of the Λ_c^+ candidate in the e^+e^- c.m. system. A Λ_c^+ candidate is accepted with $M_{\text{BC}} > 2.25$ GeV/c^2 and $|\Delta E| < 20$ MeV (corresponding to 3 times the resolution). For a given signal mode, we accept only one candidate per Λ_c charge per event. If multiple candidates are found, the one with the smallest $|\Delta E|$ is selected. The ΔE sideband region, $40 < |\Delta E| < 60$ MeV, is defined to investigate potential backgrounds.

For the $\Lambda_c^+ \rightarrow p\pi^+\pi^-$ decay, we reject K_S^0 and Λ candidates by requiring $|M_{\pi^+\pi^-} - M_{K_S^0}^{\text{PDG}}| > 15$ MeV/c^2 and $|M_{p\pi^-} - M_{\Lambda}^{\text{PDG}}| > 6$ MeV/c^2 , corresponding to 3 times the resolution, where $M_{K_S^0}^{\text{PDG}}$ (M_{Λ}^{PDG}) is the K_S^0 (Λ) mass quoted from the PDG [16] and $M_{\pi^+\pi^-}$ ($M_{p\pi^-}$) is the $\pi^+\pi^-$ ($p\pi^-$) invariant mass. These requirements suppress the peaking backgrounds of the CF decays $\Lambda_c^+ \rightarrow \Lambda\pi^+$ and $\Lambda_c^+ \rightarrow pK_S^0$, which have the same final state as the signal.

With the above selection criteria, the M_{BC} distributions are depicted in Fig. 1 for the decays $\Lambda_c^+ \rightarrow pK^-\pi^+$ and $\Lambda_c^+ \rightarrow p\pi^+\pi^-$ and in Fig. 2 (a) for the decay

$\Lambda_c^+ \rightarrow pK^+K^-$. Prominent Λ_c^+ signals are observed. The inclusive MC samples are used to study potential backgrounds. For the decays $\Lambda_c^+ \rightarrow pK^-\pi^+$ and $\Lambda_c^+ \rightarrow pK^+K^-$, no peaking background is evidenced in the M_{BC} distributions, while for the decay $\Lambda_c^+ \rightarrow p\pi^+\pi^-$, the peaking backgrounds of 28.2 ± 1.6 events from the decays $\Lambda_c^+ \rightarrow \Lambda\pi^+$ and $\Lambda_c^+ \rightarrow pK_S^0$ are expected, where the uncertainty comes from the measured BF's in Ref. [15]. The cross feed between the decay modes is negligible by the MC studies.

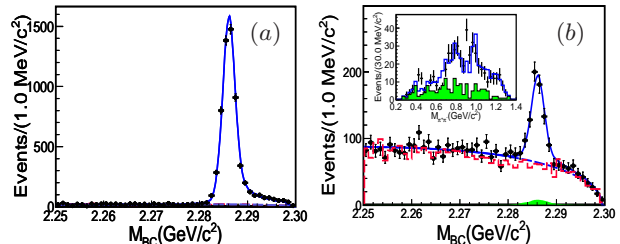


FIG. 1. Distributions of M_{BC} for the decays (a) $\Lambda_c^+ \rightarrow pK^-\pi^+$ and (b) $\Lambda_c^+ \rightarrow p\pi^+\pi^-$. Points with an error bar are data, the blue solid lines show the total fits, the blue long dashed lines are the combinatorial background shapes, and the red long dashed histograms are data from the ΔE sideband region for comparison. In (b), the green shaded histogram is the peaking background from the CF decays $\Lambda_c^+ \rightarrow pK_S^0$ and $\Lambda_c^+ \rightarrow \Lambda\pi^+$. The inset plot in (b) shows the $\pi^+\pi^-$ invariant mass distribution with the additional requirement $|\Delta E| < 8$ MeV and $2.2836 < M_{\text{BC}} < 2.2894$ GeV/c^2 , where the dots with an error bar are for the data, the blue solid histogram shows the fit curve from PWA, and the green shaded histogram shows background estimated from the M_{BC} sideband region.

To obtain the signal yields of the decays $\Lambda_c^+ \rightarrow pK^-\pi^+$ and $\Lambda_c^+ \rightarrow p\pi^+\pi^-$, a maximum likelihood fit is performed to the corresponding M_{BC} distributions. The signal shape is modeled with the MC simulated shape convoluted with a Gaussian function representing the resolution difference and potential mass shift between the data and MC simulation. The combinatorial background is modeled by an ARGUS function [23]. In the decay $\Lambda_c^+ \rightarrow p\pi^+\pi^-$, the peaking background is included in the fit, and is modeled with the MC simulated shape convoluted with the same Gaussian function for the signal, while the magnitude is fixed to the MC prediction. The fit curves are shown in Fig. 1. The M_{BC} distribution for events in the ΔE sideband region is also shown in Fig. 1(b), and a good agreement with the fitted background shape is indicated. The signal yields are summarized in Table I.

For the decay $\Lambda_c^+ \rightarrow pK^+K^-$, a prominent ϕ signal is observed in the $M_{K^+K^-}$ distribution, as shown in Fig. 2 (b). To determine the signal yields via ϕ (N_{sig}^ϕ) and non- ϕ ($N_{\text{sig}}^{\text{non-}\phi}$) processes and to better model the background, we perform a two-dimensional unbinned extended maximum likelihood fit to the M_{BC} versus $M_{K^+K^-}$ distributions for events in the ΔE signal region and side-

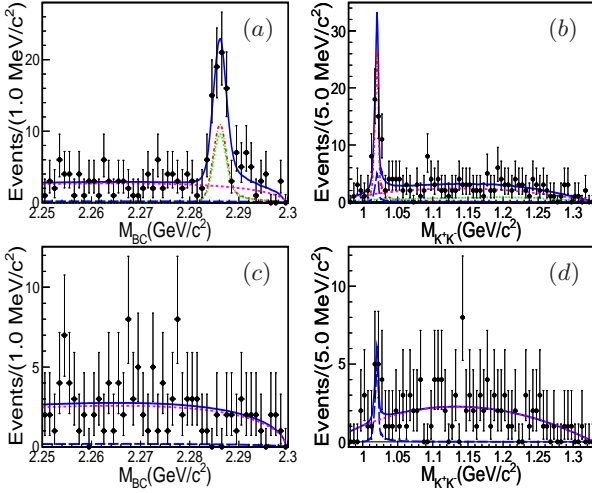


FIG. 2. Distributions of M_{BC} (left) and M_{K+K^-} (right) for data in the ΔE signal region (upper) and sideband region (bottom) for the decay $\Lambda_c^+ \rightarrow pK^+K^-$. The blue solid curves are for the total fit results, the red dash-dotted curves show the $\Lambda_c^+ \rightarrow p\phi \rightarrow pK^+K^-$ signal, the green dotted curves show the $\Lambda_c^+ \rightarrow pK^+K^-_{\text{non-}\phi}$ signal, the blue long-dashed curves are the background with ϕ production, and the magenta dashed curves are the non- ϕ background.

band region simultaneously. In the M_{BC} distribution, the shapes of Λ_c signal (via ϕ or non- ϕ process) and background, denoted as $S_{M_{BC}}$ and $B_{M_{BC}}$, respectively, are modeled similarly to those in the decay $\Lambda_c^+ \rightarrow p\pi^+\pi^-$. In the M_{K+K^-} distribution, the ϕ shape for the Λ_c process ($\Lambda_c^+ \rightarrow p\phi \rightarrow pK^+K^-$), $S_{M_{KK}}^\phi$, is modeled with a relativistic Breit-Wigner function convoluted with a Gaussian function representing the detector resolution, while that for the Λ_c decay without ϕ ($\Lambda_c^+ \rightarrow pK^+K^-$), $S_{M_{KK}}^{\text{non-}\phi}$, is represented by the MC shape with a uniform distribution in K^+K^- phase space. The shape for the non- Λ_c background including ϕ state, $B_{M_{KK}}^\phi$, has the same parameters as $S_{M_{KK}}^\phi$, while that for the background without ϕ , $B_{M_{KK}}^{\text{non-}\phi}$, is described by a third-order polynomial function. Detailed MC studies indicate the non- Λ_c background (both with and without ϕ included) have the same shapes and yields in both the ΔE signal and sideband regions, where the yields are denoted as N_{bkg}^ϕ and $N_{\text{bkg}}^{\text{non-}\phi}$, respectively. The likelihoods for the events in the ΔE signal and sideband regions are given in Eqs. (1) and (2), respectively:

$$\mathcal{L}_{\text{sig}} = \frac{e^{-(N_{\text{sig}}^\phi + N_{\text{sig}}^{\text{non-}\phi} + N_{\text{bkg}}^\phi + N_{\text{bkg}}^{\text{non-}\phi})}}{N_{\text{sig}}!} \times \prod_{i=1}^{N_{\text{sig}}} [N_{\text{sig}}^\phi S_{M_{BC}}(M_{BC}^i) \times S_{M_{KK}}^\phi(M_{K+K^-}^i) + N_{\text{sig}}^{\text{non-}\phi} S_{M_{BC}}(M_{BC}^i) \times S_{M_{KK}}^{\text{non-}\phi}(M_{K+K^-}^i) + N_{\text{bkg}}^\phi B_{M_{BC}}(M_{BC}^i) \times B_{M_{KK}}^\phi(M_{K+K^-}^i) + N_{\text{bkg}}^{\text{non-}\phi} B_{M_{BC}}(M_{BC}^i) \times B_{M_{KK}}^{\text{non-}\phi}(M_{K+K^-}^i)], \quad (1)$$

$$\mathcal{L}_{\text{side}} = \frac{e^{-(N_{\text{bkg}}^\phi + N_{\text{bkg}}^{\text{non-}\phi})}}{N_{\text{side}}!} \times \prod_{i=1}^{N_{\text{side}}} [N_{\text{bkg}}^\phi B_{M_{BC}}(M_{BC}^i) \times B_{M_{KK}}^\phi(M_{K+K^-}^i) + N_{\text{bkg}}^{\text{non-}\phi} B_{M_{BC}}(M_{BC}^i) \times B_{M_{KK}}^{\text{non-}\phi}(M_{K+K^-}^i)], \quad (2)$$

where the parameter N_{sig} (N_{side}) is the total number of selected candidates in the ΔE signal (sideband) region and M_{BC}^i and $M_{K+K^-}^i$ are the values of M_{BC} and M_{K+K^-} , respectively, for the i th event. We use the product of PDFs, since the M_{BC} and M_{K+K^-} are verified to be uncorrelated for each component by MC simulations.

The signal yields are extracted by minimizing the negative log-likelihood $-\ln \mathcal{L} = (-\ln \mathcal{L}_{\text{sig}}) + (-\ln \mathcal{L}_{\text{side}})$. The fit curves are shown in Fig. 2, and the yields are listed in Table I. The significance is estimated by comparing the likelihood values with and without the signal components included, incorporating with the change of the number of free parameters, listed in Table I.

TABLE I. Summary of signal yields in data (N_{signal}), detection efficiencies (ε), and the significances. The errors are statistical only.

Decay modes	N_{signal}	$\varepsilon(\%)$	Significance
$\Lambda_c^+ \rightarrow pK^-\pi^+$	5940 ± 85	48.0 ± 0.1	-
$\Lambda_c^+ \rightarrow p\pi^+\pi^-$	495 ± 35	59.7 ± 0.1	16.2σ
$\Lambda_c^+ \rightarrow pK^+K^-$ (via ϕ)	44 ± 8	40.2 ± 0.1	9.6σ
$\Lambda_c^+ \rightarrow pK^+K^-$ (non- ϕ)	38 ± 9	32.7 ± 0.1	5.4σ

In the decays $\Lambda_c^+ \rightarrow pK^-\pi^+$ and $\Lambda_c^+ \rightarrow p\pi^+\pi^-$, the detection efficiencies are estimated with data-driven MC samples generated according to the results of a simple partial wave analysis (PWA) by the covariant helicity coupling amplitude [24, 25] for the quasi-two-body decays. In the decay $\Lambda_c^+ \rightarrow p\pi^+\pi^-$, prominent structures arising from $\rho^0(770)$ and $f_0(980)$ resonances are observed in the $M_{\pi^+\pi^-}$ distribution as shown in the inset plot of Fig. 1(b) and are included in the PWA. Because of the limited statistics and relatively high background, the PWA does not allow for a reliable extraction of BFs for

intermediate states; it however does describe the kinematics well, and it is reasonable for the estimation of the detection efficiency. The corresponding uncertainty is taken into account as a systematic error. For the decays $\Lambda_c^+ \rightarrow pK^+K^-$ via ϕ or non- ϕ , the detection efficiencies are estimated with phase space MC samples, where the angular distribution of the decay $\phi \rightarrow K^+K^-$ is considered.

We measure the relative BFs of the SCS decays with respect to that of the CF decay $\Lambda_c^+ \rightarrow pK^-\pi^+$ and the absolute BFs by incorporating $\mathcal{B}(\Lambda_c^+ \rightarrow pK^-\pi^+) = (5.84 \pm 0.27 \pm 0.23)\%$ from the most recent BESIII measurement [15]. Several sources of systematic uncertainty, including tracking and PID efficiencies and the total number of $\Lambda_c^+\bar{\Lambda}_c^-$ pairs in the data, cancel when calculating the ratio of BFs, due to the similar kinematics between the SCS and CF decays. When calculating these uncertainties, cancellation has been taken into account whenever possible.

TABLE II. The systematic uncertainties (in percent) in the relative BF measurements. The uncertainty of the reference BF \mathcal{B}_{ref} applies only to the absolute BF measurements.

Sources	$\Lambda_c^+ \rightarrow p\pi^+\pi^-$	$\Lambda_c^+ \rightarrow p\phi$	$\Lambda_c^+ \rightarrow pK^+K^-_{\text{non-}\phi}$
Tracking	1.1	2.6	1.6
PID	1.3	1.5	1.9
V_r requirement	0.6	2.5	2.5
K_S^0/Λ vetoes	0.7	—	—
ΔE requirement	0.5	0.7	0.9
Fit	2.7	5.8	6.6
Cited branching ratio	—	1.0	—
MC model	1.4	1.0	1.1
MC statistics	0.3	0.4	0.4
Total	3.7	7.2	7.6
\mathcal{B}_{ref}	6.1	6.1	6.1

The uncertainties associated with tracking and PID efficiencies for π , K , and proton are studied as a function of (transverse) momentum with samples of $e^+e^- \rightarrow \pi^+\pi^-\pi^+\pi^-$, $K^+K^-\pi^+\pi^-$ and $p\bar{p}\pi^+\pi^-$ from data taken at $\sqrt{s} > 4.0$ GeV. To extract the tracking efficiency for particle i ($i = \pi, K$, or pton), we select the corresponding samples by missing particle i with high purity, and the ratio to find the track i around the missing direction is the tracking efficiency. Similarly, we select the control sample without a PID requirement for particle i , and then the PID requirement is further implemented. The PID efficiency is the ratio between the number of candidates with and without the PID requirement. The differences on the efficiency between the data and MC simulation weighted by the (transverse) momentum according to the data are assigned as uncertainties.

The uncertainties due to the V_r requirements and K_S^0/Λ vetoes (in $\Lambda_c^+ \rightarrow p\pi^+\pi^-$ only) are investigated by repeating the analysis with alternative requirements ($V_r < 0.25$ cm, $|M_{\pi^+\pi^-} - M_{K_S^0}^{\text{PDG}}| > 20$ MeV/ c^2 , and $|M_{p\pi^-} - M_{\Lambda}^{\text{PDG}}| > 8$ MeV/ c^2 , respectively). The result-

ing differences in the BFs are taken as the uncertainties. Uncertainties related to the ΔE resolution are estimated by widening the ΔE windows from 3σ to 4σ of the resolution.

For the decays $\Lambda_c^+ \rightarrow pK^-\pi^+$ and $\Lambda_c^+ \rightarrow p\pi^+\pi^-$, the signal yields are determined from fits to the M_{BC} distributions. Alternative fits are carried out by varying the fit range, signal shape, background shape and the expected number of peaking backgrounds. The resultant changes in the BFs are taken as uncertainties. In the decay $\Lambda_c^+ \rightarrow pK^+K^-$, the uncertainties associated with the fit are studied by varying the fit ranges, signal and background shapes for both the M_{BC} and $M_{K^+K^-}$ distributions, and ΔE sideband region.

The following four aspects are considered for the MC simulation model uncertainty. (a) The uncertainties related to the beam energy spread are investigated by changing its value in the simulation by ± 0.4 MeV, where the nominal values is 1.5 MeV determined by the data. The larger change in the measurement is taken as a systematic uncertainty. (b) The uncertainties associated with the input line shape of the $e^+e^- \rightarrow \Lambda_c^+\bar{\Lambda}_c^-$ cross section is estimated by replacing the line shape directly from BESIII data with that from Ref. [26]. (c) The Λ_c^+ polar angle distribution in the e^+e^- rest frame is parameterized with $1 + \alpha \cos^2 \theta$, where the α value is extracted from the data. The uncertainties due to the Λ_c^+ polar angle distribution are estimated by changing the α value by one standard deviation. (d) The decays $\Lambda_c^+ \rightarrow pK^-\pi^+$ and $\Lambda_c^+ \rightarrow p\pi^+\pi^-$ are modeled by a data-driven method according to PWA results. The corresponding uncertainties are estimated by changing the intermediate states included, changing the parameters of the intermediate states by one standard deviation quoted in the PDG [16], and varying the background treatment in the PWA and the output parameters for the coupling. Assuming all of the above PWA uncertainties are independent, the uncertainty related to MC modeling is the quadratic sum of all individual values. For the non- ϕ decay $\Lambda_c^+ \rightarrow pK^+K^-$, phase space MC samples with an S wave for the K^+K^- pair are used to estimate the detection efficiency. An alternative MC sample with a P wave between the K^+K^- pair is also used, and the resultant difference in efficiency is taken as the uncertainty. The uncertainties due to limited MC statistics in both the measured and reference modes are taken into account.

Assuming all uncertainties, summarized in Table II, are independent, the total uncertainties in the relative BF measurements are obtained by adding the individual uncertainties in quadrature. For the absolute BF measurements, the uncertainty due to the reference BF $\mathcal{B}_{\text{ref}}(\Lambda_c^+ \rightarrow pK^-\pi^+)$, listed in Table II, too, is included.

In summary, based on 567 pb $^{-1}$ of e^+e^- annihilation data collected at $\sqrt{s} = 4.599$ GeV with the BESIII detector, we present the first observation of the SCS decays $\Lambda_c^+ \rightarrow p\pi^+\pi^-$ and improved (or comparable) measurements of the $\Lambda_c^+ \rightarrow p\phi$ and $\Lambda_c^+ \rightarrow pK^+K^-_{\text{non-}\phi}$ BFs comparing to PDG values [16]. The relative BFs with

TABLE III. Summary of relative and absolute BFs, and comparing with the results from PDG [16]. Uncertainties are statistical, experimental systematic, and reference mode uncertainty, respectively.

Decay modes	$\mathcal{B}_{\text{mode}}/\mathcal{B}_{\text{ref}}$ (This work)	$\mathcal{B}_{\text{mode}}/\mathcal{B}_{\text{ref}}$ (PDG average)
$\Lambda_c^+ \rightarrow p\pi^+\pi^-$	$(6.70 \pm 0.48 \pm 0.25) \times 10^{-2}$	$(6.9 \pm 3.6) \times 10^{-2}$
$\Lambda_c^+ \rightarrow p\phi$	$(1.81 \pm 0.33 \pm 0.13) \times 10^{-2}$	$(1.64 \pm 0.32) \times 10^{-2}$
$\Lambda_c^+ \rightarrow pK^+K^-$ (non- ϕ)	$(9.36 \pm 2.22 \pm 0.71) \times 10^{-3}$	$(7 \pm 2 \pm 2) \times 10^{-3}$
–	$\mathcal{B}_{\text{mode}}$ (This work)	$\mathcal{B}_{\text{mode}}$ (PDG average)
$\Lambda_c^+ \rightarrow p\pi^+\pi^-$	$(3.91 \pm 0.28 \pm 0.15 \pm 0.24) \times 10^{-3}$	$(3.5 \pm 2.0) \times 10^{-3}$
$\Lambda_c^+ \rightarrow p\phi$	$(1.06 \pm 0.19 \pm 0.08 \pm 0.06) \times 10^{-3}$	$(8.2 \pm 2.7) \times 10^{-4}$
$\Lambda_c^+ \rightarrow pK^+K^-$ (non- ϕ)	$(5.47 \pm 1.30 \pm 0.41 \pm 0.33) \times 10^{-4}$	$(3.5 \pm 1.7) \times 10^{-4}$

respect to the CF decay $\Lambda_c^+ \rightarrow pK^-\pi^+$ are measured. Taking $\mathcal{B}(\Lambda_c^+ \rightarrow pK^-\pi^+) = (5.84 \pm 0.27 \pm 0.23)\%$ from Ref. [15], we also obtain absolute BFs for the SCS decays. All the results are summarized in Table III. The results provide important data to understand the dynamics of Λ_c^+ decays. They especially help to distinguish predictions from different theoretical models and understand contributions from factorizable effects [1].

The BESIII Collaboration thanks the staff of BEPCII, the IHEP computing center and the supercomputing center of USTC for their strong support. This work is supported in part by National Key Basic Research Program of China under Contract No. 2015CB856700; National Natural Science Foundation of China (NSFC) under Contracts No. 11125525, No. 11235011, No. 11322544, No. 11335008, No. 11425524, No. 11322544, No. 11375170, No. 11275189, No. 11475169, No. 11475164; the Chinese Academy of Sciences (CAS) Large-Scale Scientific Facility Program; the CAS Center for Excellence in Particle Physics (CCEPP);

the Collaborative Innovation Center for Particles and Interactions (CICPI); Joint Large-Scale Scientific Facility Funds of the NSFC and CAS under Contracts No. 11179007, No. U1232201, No. U1332201; CAS under Contracts No. KJCX2-YW-N29 and No. KJCX2-YW-N45; 100 Talents Program of CAS; INPAC and Shanghai Key Laboratory for Particle Physics and Cosmology; German Research Foundation DFG under Collaborative Research Center CContract No. RC-1044, FOR 2359; Istituto Nazionale di Fisica Nucleare, Italy; Ministry of Development of Turkey under Contract No. DPT2006K-120470; Russian Foundation for Basic Research under Contract No. 14-07-91152; U. S. Department of Energy under Contracts No. DE-FG02-04ER41291, No. DE-FG02-05ER41374, No. DE-FG02-94ER40823, No. DESC0010118; U.S. National Science Foundation; University of Groningen (RuG) and the Helmholtz Centre for Heavy Ion Research GmbH (GSI), Darmstadt; and WCU Program of National Research Foundation of Korea under Contract No. R32-2008-000-10155-0.

-
- [1] H. Y. Cheng, *Front. Phys.* **10**, 101406 (2015).
[2] C. D. Lu, W. Wang and F. S. Yu, *Phys. Rev. D* **93**, 056008 (2016).
[3] Y. Kohara, *Nuovo Cimento A* **111**, 67 (1998).
[4] M. A. Ivanov, J. G. Korner, V. E. Lyubovitskij, and A. G. Rusetsky, *Phys. Rev. D* **57**, 5632 (1998).
[5] K. K. Sharma and R. C. Verma, *Phys. Rev. D* **55**, 7067 (1997).
[6] T. Uppal, R. C. Verma, and M. P. Khanna, *Phys. Rev. D* **49**, 3417 (1994).
[7] P. Zenczykowski, *Phys. Rev. D* **50**, 402 (1994).
[8] J. G. Korner and M. Kramer, *Z. Phys. C* **55**, 659 (1992).
[9] J. G. Korner, M. Kramer, and J. Willrodt, *Z. Phys. C* **2**, 117 (1979).
[10] W. Detmold, C. Lehner, and S. Meinel, *Journal* **92**, 034503 (2015).
[11] R. Dutta, *Phys. Rev. D* **93**, 054003 (2016).
[12] G. S. Abrams *et al.* (MARKIII Collaboration), *Phys. Rev. Lett.* **44**, 10 (1980).
[13] A. M. Cnops *et al.* (BNL-0427 Collaboration), *Phys. Rev. Lett.* **42**, 197 (1979).
[14] M. Ablikim *et al.* (BESIII Collaboration), *Chin. Phys. C* **39**, 093001 (2015).
[15] M. Ablikim *et al.* (BESIII Collaboration), *Phys. Rev. Lett.* **116**, 052001 (2016).
[16] K. A. Olive *et al.* (Particle Data Group), *Chin. Phys. C* **38**, 090001 (2014).
[17] H. Y. Cheng and C. W. Chiang, *Phys. Rev. D* **81**, 074021 (2010).
[18] M. Ablikim *et al.* (BESIII Collaboration), *Nucl. Instrum. Methods Phys. Res., Sect. A* **614**, 345 (2010).
[19] S. Agostinelli *et al.*, *Nucl. Instr. Methods Phys. Res., Sect. A* **506**, 250 (2003).
[20] S. Jadach, B. F. L. Ward, and Z. Was, *Phys. Rev. D* **63**, 113009 (2001).
[21] R. G. Ping, *Chin. Phys. C* **32**, 599 (2008).
[22] D. J. Lange, *Nucl. Instrum. Methods Phys. Res., Sect. A* **462**, 152 (2001).
[23] H. Albrecht *et al.* (ARGUS Collaboration), *Phys. Lett. B* **241**, 278 (1990).
[24] S. U. Chung, *Phys. Rev. D* **57**, 431 (1998).
[25] S. U. Chung, *Phys. Rev. D* **48**, 1225 (1993).
[26] G. Pakhlova *et al.* (Belle Collaboration), *Phys. Rev. Lett.* **101**, 172001 (2008).